Assessing the probability of occurrence of earthquake-induced landslides offshore the U.S. East Coast: a first-order, second moment approach

Eugene C. Morgan[1] and Laurie G. Baise[1]

[1]Dept. of Civil and Environmental Engineering, Tufts University, 200 College Ave., Medford, MA, 02155, USA; Tel. 617 627 3098; eugene.morgan@tufts.edu

Abstract

Submarine landslides pose a direct threat to offshore infrastructure, and an indirect threat to coastal communities via tsunami generation. Recent studies have investigated the potential role that submarine landslides play in causing tsunamis on the U.S. East Coast. This paper quantitatively assesses submarine landslide hazard offshore Long Island and New Jersey, as an example, but the method herein can be applied to the entire Atlantic margin. Using publicly available bathymetry, surficial sediment data, undrained shear strength values, and earthquake ground motion predictions, we map the conditional probability of slope failure over our entire study area. We calculate this probability using a first-order, second moment estimate of the variance of critical acceleration needed to overcome the resisting forces in the infinite slope stability analysis. We show that this first-order, second moment approximation serves as a convenient and computationally efficient way of assessing submarine landslide hazard over a broad region, while also accounting for the significant uncertainties in the slope stability parameters.

1 Introduction

Recent analyses of submarine landslide hazard offshore the U.S. East Coast have focused on the potential devastation caused by tsunamis generated from such events. Earthquakes are thought to serve as the primary trigger of tsunamigenic landslides in this region. ten Brink et al. (2009) estimates the distance to the continental slope that earthquakes of various magnitudes would have to be located to trigger significantly-sized landslides. Chaytor et al. (2009) evaluate the size distribution of observed landslides along the Atlantic margin, implying trends of future activity. Grilli et al. (2009) assess submarine landslide hazard at specific locations along the upper East Coast continental slope using a Monte Carlo-based approach. The goal of this paper is to supplement these previous studies with a purely quantitative approach that incorporates a large amount of data to give a full-coverage assessment of the probability of earthquake-induced submarine landslide occurrence.

A probabilistic assessment of slope stability not only accounts for uncertainty in parameter values, but can indicate factors most responsible for destabilization as well. First-order, second moment (FOSM) analyses provide a computationally efficient way of estimating the probability of failure (Ang and Tang, 1984). This method requires a

mathematical model of failure, and mean and standard deviation values for the parameters of that model. Taking the Taylor series expansion of the model about its mean parameter values, and ignoring higher order terms, gives analytical estimates of the mean and variance of the failure metric (e.g. factor of safety (FS)). Assuming a probability distribution for FS, the mean and variance parameterize the distribution for FS, which then yields estimates of the probability of failure. Neglecting correlation between parameters in the FOSM analysis results in a much simpler expression for the variance of FS, and Haneberg (2004) notes that doing so does not significantly effect the variance estimates.

Recent studies use the FOSM method to analyze subaerial landslide hazard (Suchomel and Mašín, 2010; Chen et al., 2007; Haneberg, 2004; Giasi et al., 2003; Luzi et al., 2000), but the application of this method to submarine slope stability appears less frequently in the literature. Yang et al. (2007) compare FOSM to other probabilistic methods in evaluating the stability of a submerged, synthetic slope, and Cassidy et al. (2008) perform a retrospective FOSM analysis on a submarine slide that occurred in Finneidfjord, Norway in 1996. These studies evaluate 2-dimensional slope profiles, and we are not aware of any studies that apply the FOSM analysis over entire offshore regions.

This paper aims to provide a full-coverage, probabilistic slope stability analysis for an area covering the continental shelf and slope offshore Long Island and New Jersey. Such an analysis compliments previous studies in this area by quantitatively verifying their results while extending the assessment over the entire region and honoring publicly available data collected in the area. We show that FOSM provides an easily-implemented and reliable assessment that gives preliminary indications of potential failure "hotspots", which can then be used to direct more-detailed, future investigations.

2 Study area and data

While the entire U.S. Atlantic margin generally has good data coverage, we focus on the slope offshore Long Island and New Jersey (Figure 1a) because this area has potentially high susceptibility to tsunami run-up, and submarine mass movements have been studied here previously (e.g., Grilli et al., 2009). We expect the analysis presented here to be repeatable along the U.S. East Coast, and other offshore locations around the world with similar types of data.

The relevant data that extends over our study area includes SRTM30 global topography (and bathymetry), surficial sediment classification, undrained shear strength (s_u) values, and probabilistic peak ground accelerations. The SRTM30 dataset has a grid resolution of 30 arc seconds ($\sim$ 1km), and incorporates higher-resolution bathymetry data where available (Figure 1a). The U.S. Geological Survey (USGS) East-Coast Sediment Analysis classifies surficial sediments on the margin based on texture data and provides the interpretation as a polygon shapefile covering all of our study area (Figure 1b). Additionally, the USGS estimates s_u through a variety of methods (including lab measurements and empirical relationships), and present the values in their

usSEABED database. In order to study shallow landslides, we filter out any s_u values from depths greater than 1m below seafloor (points in Figure 1c). To assess earthquakes as a potential triggering mechanism for submarine landslides in this area, we use 2008 USGS National Seismic Hazard Maps for the East Coast which give earthquake peak ground accelerations (PGA) for various probability levels (we choose to look at the largest and rarest ground motions: 2% probability of exceedance in 50 years)(Figure 1d).

3 Data processing

In order to make the subsequent calculation outlined in the next section, we convert all the necessary data layers to a raster format. Because the SRTM30 layer provides the highest resolution, we sample the other layers onto its grid. Slope angle (α) comes from computing the directional derivative of the SRTM30 elevation data, so does not need to be re-gridded. We use literature values for the total unit weights (γ) of the surficial sediments (values listed in Table 1), and so we rasterize the surficial sediment polygons to the SRTM30 grid. The effective unit weight (γ') used in the FOSM calculations comes from subtracting the unit weight of water (9.81 kN/m^3) from the total unit weight.

Table 1: Total unit weights used for each sediment type.

Sediment	γ (kN/m^3)	σ_γ (kN/m^3)
Sand/silt/clay	15.451	0.981
Sand-silt/clay	17.364	0.981
Clay	15.696	0.981
Sand-clay/silt	17.364	0.981
Clay-silt/sand	14.519	0.981

Sediment	γ (kN/m^3)	σ_γ (kN/m^3)
Sand	18.639	0.981
Gravel-sand	18.639	1.962
Gravel	20.601	1.962
Bedrock	29.430	0.981

Gridding the usSEABED s_u values is more difficult because these data exist at discrete points. We interpolate these values to the SRTM30 grid by means of stratified kriging (base layer in Figure 1c). Stratified kriging differs from ordinary kriging in that it predicts s_u values only at grid cells that belong to the same surficial sediment unit as the data points. That is, this type of kriging stratifies the s_u data points by the sediment type they lie within, builds sample variograms from the stratified data, fits a variogram model to each variogram, and then predicts within each sediment unit based on the unit's respective model. Not only does the model honor (potential) differences in spatial correlation structure between sediment types, but will help mitigate the bias arising from denser s_u sampling near-shore. Also, kriging gives uncertainties (variances) with its predictions, making it compatible in providing parameters for the FOSM method.

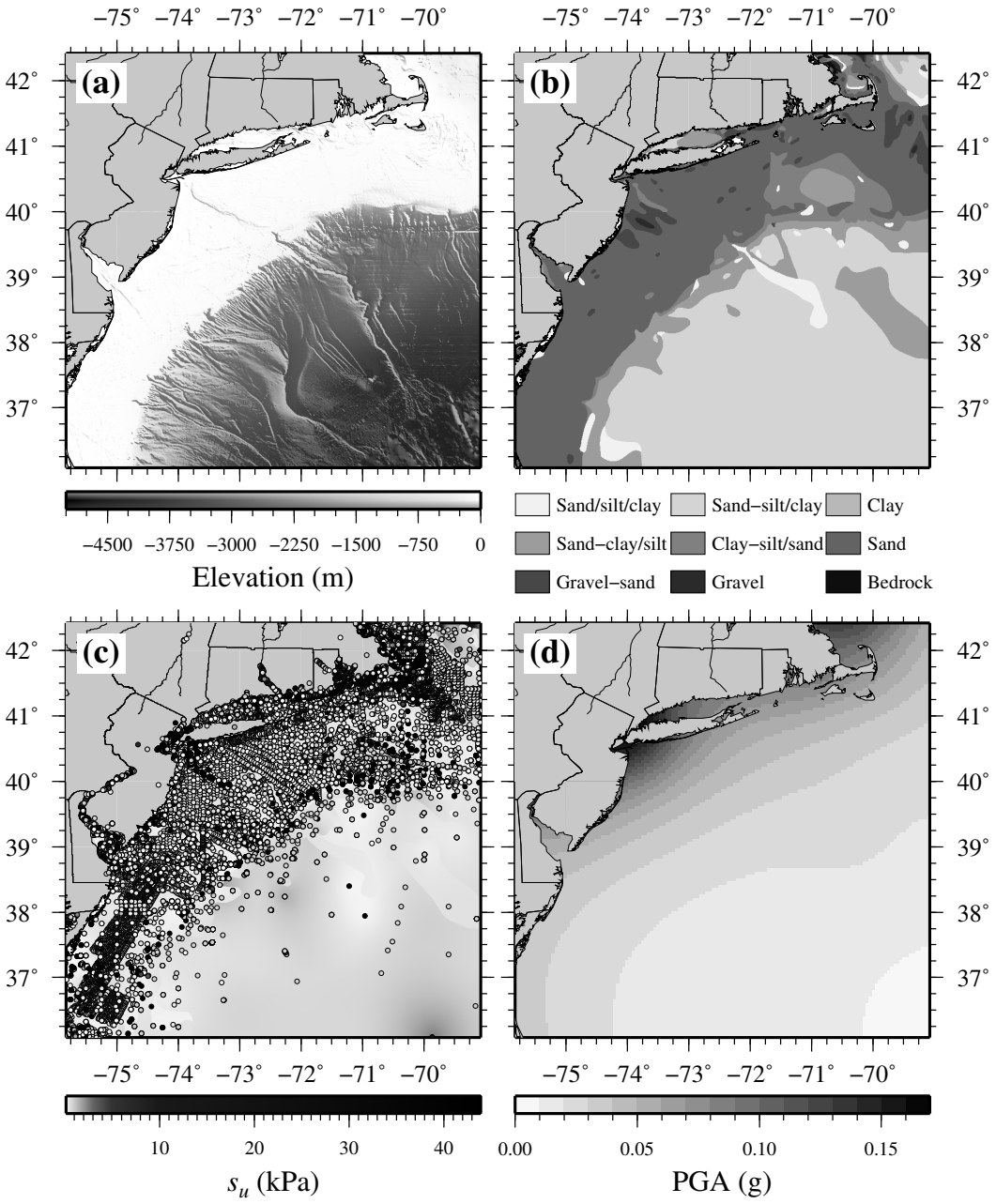

Figure 1: Location of study area, displaying a) SRTM30 bathymetry, b) East-Coast Sediment Analysis surficial sediment classifications, c) usSEABED s_u values within 1m below seafloor on top of the kriged s_u values, and d) peak ground acceleration (PGA) with 2% probability of exceedance in 50 years.

4 FOSM for FS and a_c

In our infinite slope stability analysis, we parameterize all the resisting forces with the undrained shear strength (s_u) given by the usSEABED dataset. Our static factor of safety is then $FS = s_u/(\gamma' z \sin\alpha \cos\alpha)$, where the driving force in the denominator

results from the buoyant weight of the soil mass (γ' times thickness z) on the slope with angle α. For the FOSM method, we take the partial derivatives of FS with respect to s_u and γ', giving $\partial FS/\partial s_u = (\csc\alpha\sec\alpha)/(\gamma' z)$, and $\partial FS/\partial\gamma' = (-s_u \csc\alpha\sec\alpha)/(\gamma'^2 z)$. Here, we only take the derivatives with respect to s_u and γ' because we assume that these two parameters contain all the uncertainty in FS; we measure α directly from the SRTM30 bathymetry and arbitrarily evaluate shallow-seated slides with $z = 1$m. Our mean FS estimate (mapped in Figure 2a) comes from evaluating the equation for FS at the mean parameter values ($\bar{x}_i = (\bar{s}_u, \bar{\gamma}')$), while the variance of FS (σ^2_{FS}) comes from evaluating $\sigma^2_{FS} = \sum_i (\partial FS/\partial x_i)^2_{\bar{x}_i} \sigma^2_{x_i}$, where $\sigma^2_{x_i}$ is the vector of variances for $x_1 = s_u$ and $x_2 = \gamma'$. Figure 2b shows the static factor of safety standard deviation σ_{FS}.

We can repeat the FOSM method for the critical acceleration a_c, which includes the static factor of safety $a_c = (FS-1)g\sin\alpha = s_u g/(\gamma' z\cos\alpha) - g\sin\alpha$, where g is gravity (Newmark, 1965). Taking the partial derivatives gives $\partial a_c/\partial s_u = (g\sec\alpha)/(\gamma' z)$, and $\partial a_c/\partial\gamma' = (-s_u g\sec\alpha)/(\gamma'^2 z)$. Again, our mean a_c estimate (Figure 2c) comes from evaluating the equation for a_c above at the mean parameter values, and $\sigma^2_{a_c} = \sum_i (\partial a_c/\partial x_i)^2_{\bar{x}_i} \sigma^2_{x_i}$. Figure 2d shows the critical acceleration standard deviation σ_{a_c} in order to keep the units comparable to the a_c values. We can then calculate the probability of failure (P[fail], Figure 3) by parameterizing the normal cumulative distribution function with a mean equal to a_c and a standard deviation equal to σ_{a_c}, and plugging in the mapped PGA values (Figure 1d). In other words, P[fail] is the area of the normal density curve centered at $\bar{a}_c$ with standard deviation σ_{a_c} that lies below the given PGA value. Therefore, keep in mind that the probabilities of failure plotted in Figure 3 are conditional on the PGAs with 2% probability of exceedance in 50 years, which are the rarest (and thus largest) predictions of ground motion available from the USGS.

5 Discussion

While areas of higher landslide hazard largely exist on steeper slopes, α is not the only variable controlling the distribution of failure probabilities in Figure 3. We see from Figure 2 that the lowest FS and a_c generally occur on the upper portion of the continental slope, which has the steepest slopes ($2^\circ < \alpha < 53^\circ$), with the largest α occurring in incisions in the slope. From Figure 3, we see the largest P[fail] values ($> 50\%$) share the same association, but a strict causative relationship between α and P[fail] cannot be made; numerous patches of P[fail] $< 50\%$ exist on the upper slope and some patches of P[fail] $> 50\%$ have shallow slope angles. While the upper slope largely contains sand-clay/silt with sand-silt/clay draping the lower slope and patches of sand/silt/clay, the lower probabilities are primarily associated with clay-silt/sand, which is lighter than the former three sediment types. Additionally, s_u has a strong influence on the spatial variation of P[fail] within the continental shelf.

Figure 3 identifies specific areas of distinctly high landslide hazard. A small patch to the south on the upper slope (around -74.75°, 36.25°) has P[fail] $> 80\%$, which is surrounded by significantly smaller probabilities. Large patches of higher probability exist off Delaware, owing to localized spots of low s_u and higher levels of ground motion. Additionally, the canyon incised by the Hudson river (below Long Island) hosts

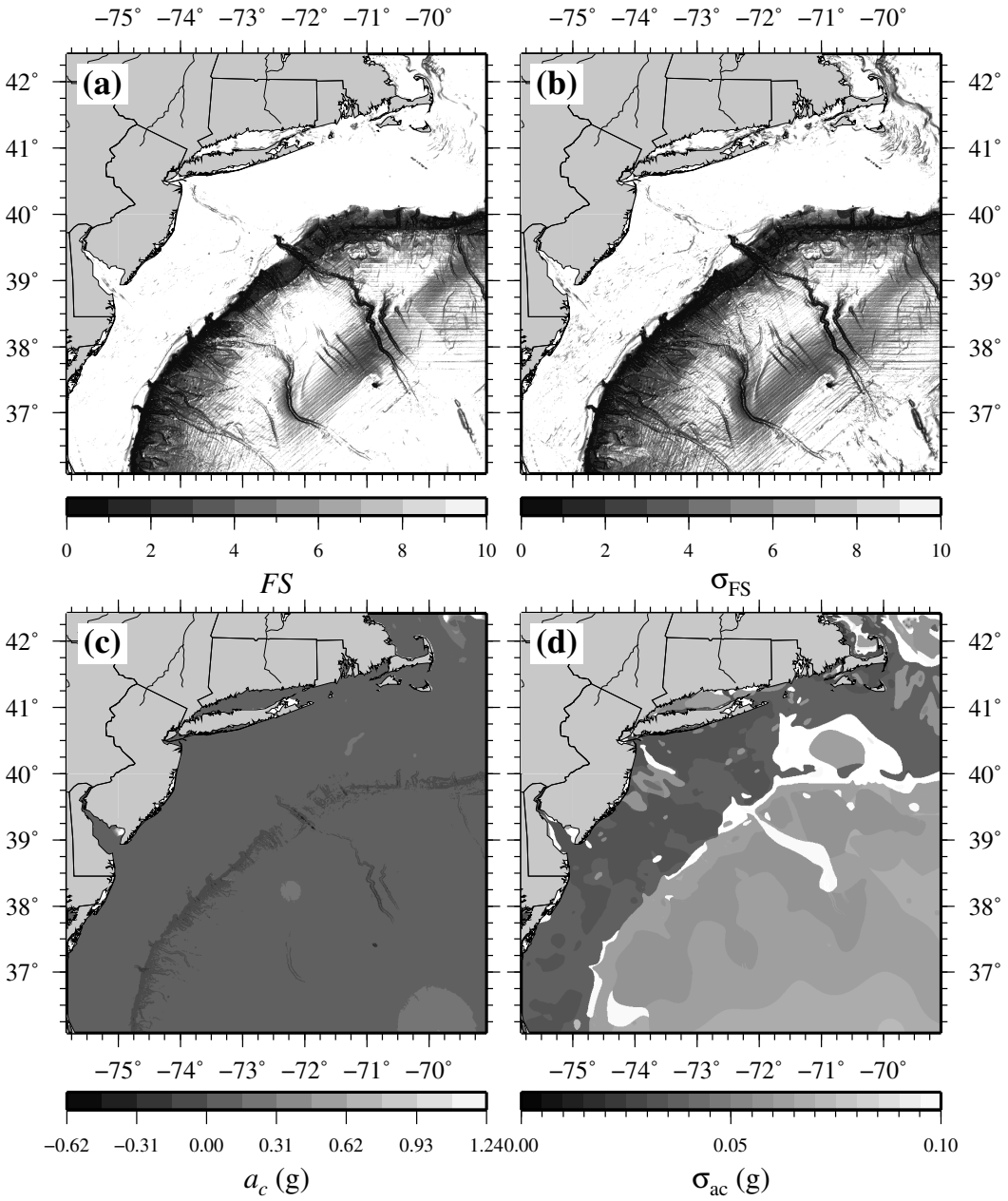

Figure 2: Results from the FOSM analysis with input data from Figure 1 and Table 1: a) static factor of safety FS clipped to values ≤ 10, b) standard deviation of static factor of safety σ_{FS}, also clipped to values ≤ 10, c) critical acceleration a_c, and d) σ_{a_c}. Note that negative a_c values are associated with $Fs < 1$. Values are shaded by the SRTM30 terrain to show their relationship to geomorphic features.

higher probabilities than neighboring areas on the lower slope, but these hazardous areas do not extend beyond the canyon walls. In general, canyons in the slope host markedly higher probabilities of failure, and should be investigated in greater detail.

It is also important to note that the higher $P[\text{fail}]$ values co-locate with negative a_c

values on the continental slope, which in turn are associated with $FS < 1$. Even though the locations with $FS < 1$ have relatively low uncertainty ($\sigma_{FS} < 1$), they also lie in sparser s_u data coverage, so the shear strength of these slope sediments are not nearly as well-characterized as on the shelf. Similarly, using arbitrarily different γ values may reduce the distribution of $FS < 1$. Also, while the $FS < 1$ values generally have smaller uncertainty than larger FS values, negative a_c values have larger or just as large σ_{a_c} values as areas with larger a_c values. Namely, in Figure 2d, the upper slope generally has larger uncertainty (σ_{a_c}) than either the lower slope or shelf. Thus, we are not as confident in our estimates of the most hazardous areas as we are in the least hazardous areas.

6 Conclusion

While this study presents some significant findings, certain limitations in the analysis have yet to be overcome. For one, this analysis does not account for earthquake duration (i.e. Arias intensity) and Newmark displacements, which determine whether slope material will fail catastrophically or not. Exceeding a_c may cause the soil mass to slip, but will the soil mass slip far enough to completely fail? Here we have limited the calculations to $z = 1$m, when it should be fairly easy to iterate the calculations over a variety of landslide thicknesses. Deeper z values add the complexity of sub-seabed structure and parameter variation with depth into the analysis, but in order to address tsunami generation, this analysis must adequately consider landslide thickness. Furthermore, our estimates of γ are rudimentary at best, and having field measurements of γ would improve the results significantly.

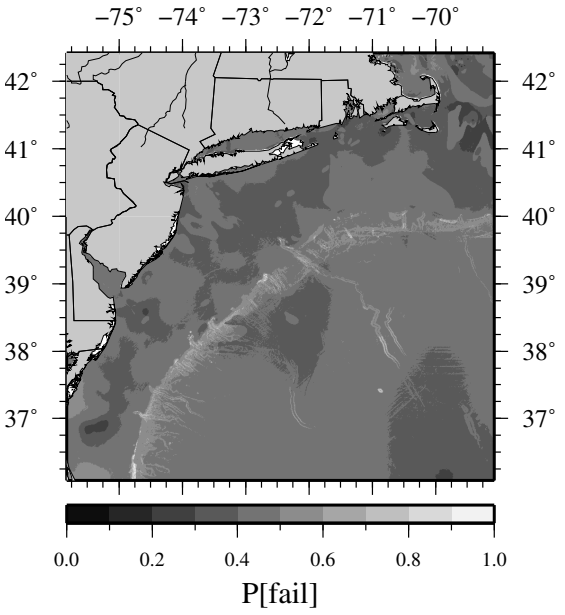

Figure 3: The probability of shallow slope failure given the peak ground accelerations with 2% probability of exceedance in 50 years (Figure 1d).

Despite the above limitations, this paper illustrates the viability of the FOSM method as a preliminary indicator of the most hazardous areas in an entire region. Via FOSM analysis, one can easily construct an analytical expression for the uncertainty of a chosen failure metric, thus easing the computation of failure probabilities from a large amount of data.

References

Ang, A. H.-S., Tang, W. H., 1984. Probability Concepts in Engineering Planning and Design. J. Wiley & Sons, New York (etc...).

Cassidy, M. J., Uzielli, M., Lacasse, S., SEP 2008. Probability risk assessment of landslides: A case study at Finneidfjord. Canadian Geotechnical Journal 45 (9), 1250–1267.

Chaytor, J. D., ten Brink, U. S., Solow, A. R., Andrews, B. D., 2009. Size distribution of submarine landslides along the us atlantic margin. Marine Geology 264 (1-2), 16–27.

Chen, J. C., Jan, C. D., Lee, M. H., 2007. Probabilistic analysis of landslide potential of an inclined uniform soil layer of infinite length: theorem. Environmental Geology 51 (7), 1239–1248.

Giasi, C. I., Masi, P., Cherubini, C., 2003. Probabilistic and fuzzy reliability analysis of a sample slope near aliano. Engineering Geology 67 (3-4), 391 – 402.

Grilli, S. T., Taylor, O. D. S., Baxter, C. D. P., Maretzki, S., 2009. A probabilistic approach for determining submarine landslide tsunami hazard along the upper east coast of the united states. Marine Geology 264 (1-2), 74–97.

Haneberg, W. C., 2004. A rational probabilistic method for spatially distributed landslide hazard assessment. Environmental & Engineering Geoscience 10 (1), 27–43.

Luzi, L., Pergalani, F., Terlien, M. T. J., 2000. Slope vulnerability to earthquakes at subregional scale, using probabilistic techniques and geographic information systems. Engineering Geology 58 (3-4), 313–336.

Newmark, N. M., 1965. Effects of earthquakes on dams and embankments. Geotechnique 15 (2), 139–160.

Suchomel, R., Mašín, D., 2010. Comparison of different probabilistic methods for predicting stability of a slope in spatially variable c-ϕ soil. Computers and Geotechnics 37 (1-2), 132 – 140.

ten Brink, U. S., Lee, H. J., Geist, E. L., Twichell, D., 2009. Assessment of tsunami hazard to the u.s. east coast using relationships between submarine landslides and earthquakes. Marine Geology 264 (1-2), 65 – 73.

Yang, S., Nadim, F., Forsberg, C., 2007. Probability study on submarine slope stability. In: Lykousis, V., Sakellariou, D., Locat, J. (Eds.), Submarine Mass Movements and Their Consequences. Vol. 27 of Advances in Natural and Technological Hazards Research. Springer Netherlands, pp. 161–170, 10.1007/978-1-4020-6512-5_17.